Fluorescence suppression using wavelength modulated Raman spectroscopy in fiber-probe-based tissue analysis

Bavishna B. Praveen
Praveen C. Ashok
Michael Mazilu
Andrew Riches
Simon Herrington
Kishan Dholakia

Fluorescence suppression using wavelength modulated Raman spectroscopy in fiber-probe-based tissue analysis

Bavishna B. Praveen,[a*] **Praveen C. Ashok,**[a*] **Michael Mazilu,**[a] **Andrew Riches,**[b] **Simon Herrington,**[b] **and Kishan Dholakia**[a]
[a]University of St Andrews, SUPA, School of Physics & Astronomy, North Haugh, St Andrews, Fife, Scotland, KY16 9SS, United Kingdom
[b]University of St Andrews, School of Medicine, Medical and Biological Sciences Building, North Haugh, St Andrews, KY16 9TF, United Kingdom

Abstract. In the field of biomedical optics, Raman spectroscopy is a powerful tool for probing the chemical composition of biological samples. In particular, fiber Raman probes play a crucial role for *in vivo* and *ex vivo* tissue analysis. However, the high-fluorescence background typically contributed by the auto fluorescence from both a tissue sample and the fiber-probe interferes strongly with the relatively weak Raman signal. Here we demonstrate the implementation of wavelength-modulated Raman spectroscopy (WMRS) to suppress the fluorescence background while analyzing tissues using fiber Raman probes. We have observed a significant signal-to-noise ratio enhancement in the Raman bands of bone tissue, which have a relatively high fluorescence background. Implementation of WMRS in fiber-probe-based bone tissue study yielded usable Raman spectra in a relatively short acquisition time (∼30 s), notably without any special sample preparation stage. Finally, we have validated its capability to suppress fluorescence on other tissue samples such as adipose tissue derived from four different species. © *2012 Society of Photo-Optical Instrumentation Engineers (SPIE).* [DOI: 10.1117/1.JBO.17.7.077006]

1 Introduction

Raman spectroscopy is a powerful spectroscopic technique that yields chemical information from a sample by the analysis of photons, which are inelastically scattered from the vibrational modes of the molecules in the sample.[1,2] While Raman spectroscopy provides high information content with regard to the chemical and the biomechanical properties of the samples, the sensitivity of this method is restricted by the background from the auto-fluorescence of the sample.[3–5] A variety of techniques such as coherent anti-stokes Raman scattering (CARS), time-resolved spectroscopy, polarization modulation, and wavelength-modulated Raman spectroscopy (WMRS) have been developed in the past three decades to recover Raman signal by suppressing unwanted background fluorescence signals.[6–12] Fluorescence suppression using wavelength modulation has remained the simplest to implement considering the extra instrumentation required.[7,8,10] Recent advancements in continuous or discrete WMRS has shown that it is even possible to obtain the difference spectra without lock-in amplification using algorithms such as principal component analysis (PCA) or expectation maximization (EM).[6,13] The applicability of these fluorescence suppression techniques in the biomedical field is still largely unexplored, although Raman spectroscopy is widely applied in the field of biomedicine owing to its non-invasive, label-free nature.[1]

The fiber-based implementation of Raman spectroscopy has been used for a variety of bio-medical applications.[14,15] A fiber probe may exploit the advantages of Raman spectroscopy along with the ability to guide light flexibly for endoscopic applications, making it an ideal candidate for *in vivo* or *ex vivo* chemical analysis of tissues.[16,17] Since Raman spectra provide a tissue-specific fingerprint of the sample, pathological changes in a tissue sample are reflected in the Raman spectra and can be subsequently used for diagnostic applications with suitable multivariate analysis.[18]

In the case of highly scattering samples such as tissues, the light beam scatters within the sample and the Raman signal (diffuse photons) itself undergoes multiple scattering, a process generally termed Raman photon migration, which causes high fluorescence background.[19] Additionally, when a fiber Raman probe is used the fiber material itself also contributes significantly to fluorescence in the fingerprint region between 400 to 2000 cm^{-1} (Ref. 18). Suppressing the fluorescence thus becomes a critical step to retrieve the weaker signals recorded using fiber-based Raman systems. Importantly, variations in the background fluorescence can affect the resultant sensitivity and specificity when classifying real biological samples.

We report here the use of WMRS for fluorescence suppression in fiber Raman probe-based tissue studies. In this technique, the excitation wavelength is slightly modulated while acquiring the Raman signal; a slight shift in the excitation wavelength shifts the Raman peaks while the background fluorescence remains a constant. This differential signal is then extracted by applying (PCA) to the data set.[13] With WMRS no specific sample preparation step is required to suppress the fluorescence background, and also this method has been shown to be highly advantageous when compared with similar methods such as shifted-excitation Raman difference spectroscopy (SERDS).[6,13]

Using WMRS *ex-vivo* Raman spectroscopic studies on bone tissue was performed. Raman spectroscopic analyses on bone tissue aim at probing the local changes in mineral composition

and the mineral/matrix ratio. These reflect aspects such as bone maturity, disease state, and degree of microscopic damage.[3,4] Several studies have been reported in the area of analyzing bone tissues using fiber-probe-based Raman system in the last decade.[4,20–24] Several studies attempted bone fluorescence suppression using various methods. This includes methods such as the treatment with hydrogen peroxide, acetone, brine, and detergents though these may compromise the integrity of the sample.[4,5] Another approach to suppress bone fluorescence utilized photo-irradiation of the tissue sample with 532-nm laser wavelength for a period ranging from 2 to 4 h, acknowledging that the sample could be damaged after the first 40 min.[3,4]

Our nondestructive method for fluorescent suppression shows an enhancement in the signal-to-noise ratio (SNR) of Raman bands in bovine bone tissue with reasonably short acquisition times (∼30 s). The reproducibility of the WMRS method is determined by retrieving the signal acquired using two different Raman probes with different fluorescence characteristics. We have implemented a procedure to simultaneously correct for power fluctuations and photo-bleaching while processing the WMRS data. Finally, we demonstrate the enhancement of the Raman signal by the implementation of WMRS within a fiber Raman probe for the study of animal fat derived from various species.

2 Experimental

2.1 Instrumentation

The experimental setup was similar to that described previously.[25] We use a tunable diode laser (Sacher, Littmann configuration, 785 nm, maximum power 1 W, total tuning range 200 GHz). The laser beam was coupled to the excitation part of the Raman probe (Emvision LLC) after passing through a line filter. The collection part of the probe was then coupled to the spectrometer (Shamrock SR-303i, Andor Technology) using an F-number matcher. The F-number of the spectrometer was 4, and that of the collection fiber was 2.27. Hence a pair of lenses with focal lengths of 16 and 10 mm, respectively were used in the F-number matcher, between which an edge filter (SEMROCK) was inserted to filter out 785 nm photons. The spectrometer was equipped with a 400 lines/mm grating with a deep depletion, back illuminated and thermo-electrically cooled CCD camera (Newton, Andor Technology).

The fiber probe used for this study had one optical fiber with a 200-μm diameter to deliver the excitation beam and seven optical fibers each of 200-μm diameter to collect the Raman signal. The excitation part in the probe head included a line filter to filter out background fluorescence from the fiber, and the collection part included a high-pass filter which rejects the 785-nm photons. A GRIN lens at the tip of the probe head helped to increase the collection efficiency. The probe had a 1-m-long fiber pigtail, and the probe head had a diameter of 4.2 mm. With a working distance of ∼1 mm, the output excitation beam from the probe at 1 mm had a diameter of ∼500 μm. In order to avoid signal fluctuations due to variation in the axial height of the probe head from the tissue surface, the probe was converted to a contact probe by introducing a sapphire window at the tip of the probe head. This was achieved by inserting the probe head into a flexible sleeve (Tygon) of inner diameter 4.8 mm, outer diameter 6.8 and length 40 mm, to the end of which a 1 mm thick sapphire window (Comar optics) was fixed. This contact probe head was pressed

against the tissue surface while acquiring Raman spectra. The average excitation power at the sample was ∼200 mW, which corresponds to a power density of ∼25 W/cm^2. In order to compare the probe performances, another custom-designed fiber probe (Emvision LLC) with a 5-m fiber pigtail length was also used to acquire Raman spectra from bone tissue. The optical design of the second fiber probe was similar to the one described previously, except for the longer fiber pigtail length, which would contribute to higher background from the fiber. Although the probe head design was similar it was experimentally observed that the longer probe had higher collection efficiency while the fluorescence background was higher due to the longer fiber pigtail.

All the data presented in this paper were acquired at a single grating position of the spectrometer. The wave-number axis was calibrated using a quadratic interpolation for four standard Raman peaks of ethanol in the fingerprint region.

2.2 Sample

The samples used for the investigation were bovine bone tissues and adipose tissue derived from chicken, pork, beef, and lamb. The bovine bone tissue was dissected from the rib of beef; the adipose tissue for the experiment was dissected adjacent to the rib of the beef, pork, and lamb. In the case of chicken, the adipose tissue was dissected from above the chicken breast, all within 48 h of slaughter.[26] Care was taken to ensure that for adipose tissue only the part next to the skin was chosen for the experiment since the fatty acid composition changes across the cross-section of the tissue.[26,27] The Raman signals from all these samples were collected at the ambient temperature of 19 to 21°C. For each sample, 20 different spectra were collected to ensure we could obtain reliable statistics.

2.3 Raman Acquisition Method

The principle of WMRS depends on the fact that, in contrast to the fluorescence background, the Raman peaks synchronously modulate along with the modulation of the excitation wavelength. This differential signal is then extracted from the constant background by using PCA, where a singular value decomposition (SVD) algorithm was used to estimate the principal components.[13] The experiment consists of acquiring a series of Raman spectra each with 5-s single exposure time; each spectra corresponds to a slightly differing excitation wavelength in discrete steps with equal intervals. Each Raman spectrum was acquired by full vertical binning (FVB) the CCD. The wavelength of the excitation beam was varied in discrete steps in a symmetric trapezoidal pattern with time period 30 s. The amplitude of the modulation was $\Delta\nu = 160$ GHz, which corresponds to a wavelength shift of $\Delta\lambda = 0.32$ nm. For the tissue analysis, the total acquisition time was 30 s corresponding to 6 spectra. The SNR of the modulated signal depends on the modulating amplitude, frequency and acquisition time, and in turn these parameters depend on the fluorescence characteristics and Raman cross-section of the sample, the shape of the Raman peak, and the detection geometry itself.[25]

From a measured dataset, a standard Raman spectrum was obtained by accumulating all modulated spectra belonging to a set.

2.4 Data Treatment

Each of the acquired spectra was normalized (as explained in the section below), and PCA was then applied to obtain the modulated Raman spectra from the constant fluorescence background. The spectrum of the first principal component corresponds with the maximum variation in the data set originating from the continuous shift of the Raman peaks. This spectrum gives a derivative-like Raman signal with most of the fluorescence background suppressed.

The standard Raman spectrum was smoothed with a Savitzky Golay filter of smoothing width 9 and order 3.

The SNR measured from the differential spectrum was compared with that from the standard Raman spectrum obtained for the same peak. The SNR of a particular Raman peak was estimated as the ratio of the peak intensity value (peak-to-peak value for modulated Raman spectra) to the standard deviation of the signal in a Raman free spectral region (here we chose 2000 to 2060 cm^{-1} as the noise region).[13] For a fair comparison between the SNR of standard and modulated Raman, SNR from the first differential of the standard Raman spectrum was also estimated. Signal to background (S/B) of a Raman peak was estimated as the ratio of the height of the Raman peak from the fluorescence background to the height of the fluorescence background,[28] after subtracting the dark current of the CCD from the recorded spectrum.

2.4.1 Correction for intensity fluctuations and photo-bleaching

The basic assumption of the WMRS technique is that only Raman peaks get shifted between different short acquisitions while the fluorescence background remains constant. In practice, this is not completely true. The power of the laser source fluctuates [~5% as shown in Fig. 1(b)] while the wavelength of the source is modulated.[7] Another source of fluctuation contained within the fluorescence background (especially when biological samples are probed) is the photo-bleaching of the sample. In order for the PCA procedure to pick out the Raman peak, both of these two fluctuations have to be corrected simultaneously.

Although photo-bleaching results in an exponentially decaying fluorescence signal, within a relatively short acquisition time (10 s), this can be corrected by subtracting the signal with a linear or second order polynomial fit. The power fluctuation can be normalized by estimating the normalization factors from the Raman free spectral region (background region).

In order to demonstrate the process of correcting for power fluctuation and photo-bleaching, a set of 36 wavelength-modulated Raman spectra, corresponding to six modulation cycles is chosen. Each spectrum is acquired with 5-s acquisition time and the dataset is represented as a 1024×36 matrix. Each column in this dataset corresponds to a single Raman spectrum and each row corresponds to variation of intensity of the spectra at a particular pixel. Without these fluctuations, a row in a Raman band region should be periodically fluctuating while a row in a background region should ideally be non-fluctuating.

Figure 1(a) to 1(h) details the correction procedure, where in each plot, one data point corresponds to the pixel intensity of a single Raman spectrum. The first step is to find the factors to correct for power fluctuation. The mean of 10 rows in the background region (10 pixels from 2000 cm^{-1} in this case) was estimated for this [Fig. 1(a)]. To separate the power fluctuation information from variation due to photo-bleaching, a second order polynomial fit was performed on this mean data.
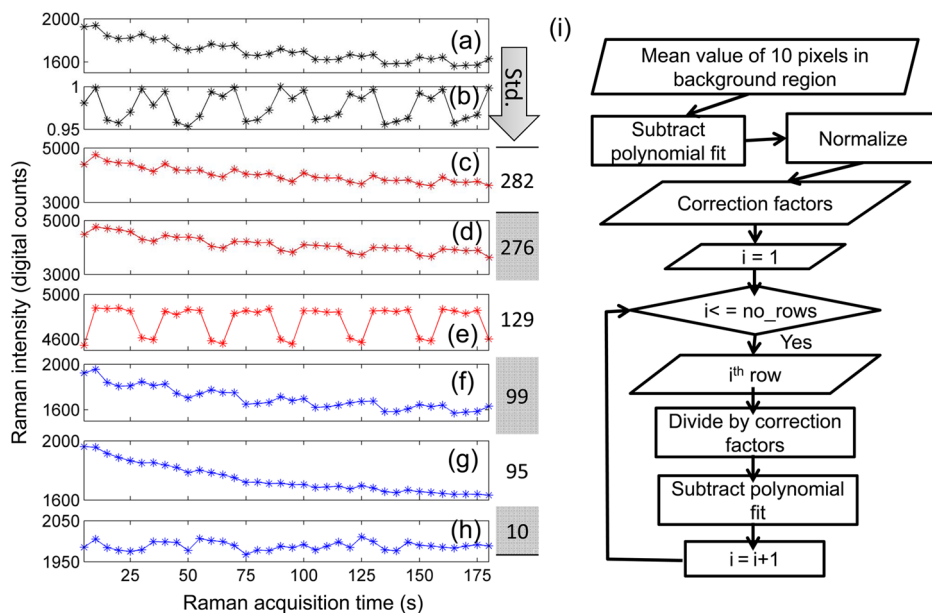

Fig. 1 Illustration of the procedure to correct the signal for power fluctuation and photo-bleaching, using a dataset of 36 Raman spectra. Each point in the plots [(a)] to [(h)] corresponds to the pixel intensity of a single Raman spectrum. (a) Mean value of adjacent 10 pixels from 2000 cm^{-1} in the noise region. (b) Normalization factors obtained from the data shown in [(a)] after correcting this data for photo-bleaching by subtracting a second order polynomial fit. (c) Variation of signal intensity of a pixel at a Raman band region. (d) Signal shown in [(c)] after normalization using the normalization factors shown in [(b)]. (e) Signal shown in [(d)] after correcting for photo-bleaching by subtracting second order polynomial fit. It can be seen that the signal periodically fluctuates which corresponds to the modulation of the wavelength of excitation. (f) Variation of signal intensity of a pixel at a noise region. (g) Signal shown in [(f)] after normalization using the normalization factors shown in [(b)]. (h) Signal shown in [(g)] after correcting for photo-bleaching subtracting a second order polynomial fit. (Std.) Standard deviation of signals. (i) flow chart showing the correction procedure.

Subsequently this fit was subtracted from this mean data. Each of the elements in this fit-subtracted data was subsequently divided with the intensity value of the 14th acquisition (chosen randomly) to obtain factors to correct for power fluctuation [Fig. 1(b)].

After obtaining the correction factors, each row in the dataset was corrected for photo-bleaching by subtracting the data with a second order polynomial fit, followed by dividing with the correction factors [Fig. 1(b)] in order to compensate for the power fluctuations.

The effect of this correction is illustrated in Fig. 1(c) to 1(h). Figure 1(c) shows a row in the region of a Raman peak. After correcting for power fluctuation the resultant data is shown in Fig. 1(d), where it can be seen that, although there is a periodicity in the signal, the signal is decaying due to the photo-bleaching effect. After correcting for photo-bleaching, the data as seen in Fig. 1(e) is periodically fluctuating. This corresponds to the wavelength modulation of the Raman peak. Figure 1(f) shows a row in a fluorescence background region. Figure 1(g) shows the data after power fluctuation corrections and Fig. 1(h) shows the data after correction for photo-bleaching. It can be seen that the ratio of standard deviation of the array in Fig. 1(e) and 1(h) is one order of magnitude higher than the ratio of standard deviation between the arrays in Fig. 1(c) and 1(f). This naturally translates into a better distinction of Raman peak and fluorescence background when PCA is applied to this series of modulated Raman spectra. The Matlab code for the correction procedure is given as an Appendix to this article.

3 Results and Discussion

3.1 Bovine Bone Tissue Fluorescence Suppression

Raman spectra of bovine bone tissue were acquired using fiber Raman probes. A comparison of the standard and modulated signals is shown in Fig. 2. It can be seen that the modulation technique has suppressed the fluorescence background and enhanced the SNR of Raman peaks. We performed this experiment with two different Raman probes of differing pig tail lengths: 1 m and 5 m. It can be seen that the signal to background ratio for the phosphate v_1 peak (marked in the figure by a star symbol) at 960 cm^{-1} is higher for the probe with the shorter fiber pigtail due to the higher fluorescence contribution from the material of the fiber. However it was observed that there was a significant enhancement (~8 times) in the phosphate ν_1 Raman peak in the modulated signal when compared with the standard for both of the fiber Raman probes. When compared with the SNR of the first order differential of the standard Raman spectrum, the phosphate ν_1 Raman peak improved the SNR by a factor of approximately two. However, the first order differential contained some artifacts in the form of spurious peaks. The higher SNR for the fiber probe with the longer fiber pigtail is due to the higher collection efficiency of that probe. With this technique even the other weak peaks at 1070 cm^{-1} corresponding to the carbonate ν_1, the amide III peak at 1245 cm^{-1}, CH$_2$ scissoring at 1451 cm^{-1}, and the amide I peak at 1672 cm^{-1} were amplified as shown in the Fig. 2.[3] The total acquisition time required to collect this signal was 30 s.

3.2 Fluorescence Suppression in Adipose Tissue

The WMRS technique may also be used to analyze samples with relatively high Raman cross-section, since WMRS can enhance the SNR of the Raman peaks. In order to demonstrate this, Raman spectra of adipose tissues from four different species—namely pig, lamb, chicken, and beef—were analyzed. The Raman spectra of the adipose tissues may be an indicator towards the quality of different animal fats.[26,27]

Figure 3 shows the standard and modulated Raman spectra acquired from adipose tissues of four species. It can be seen that
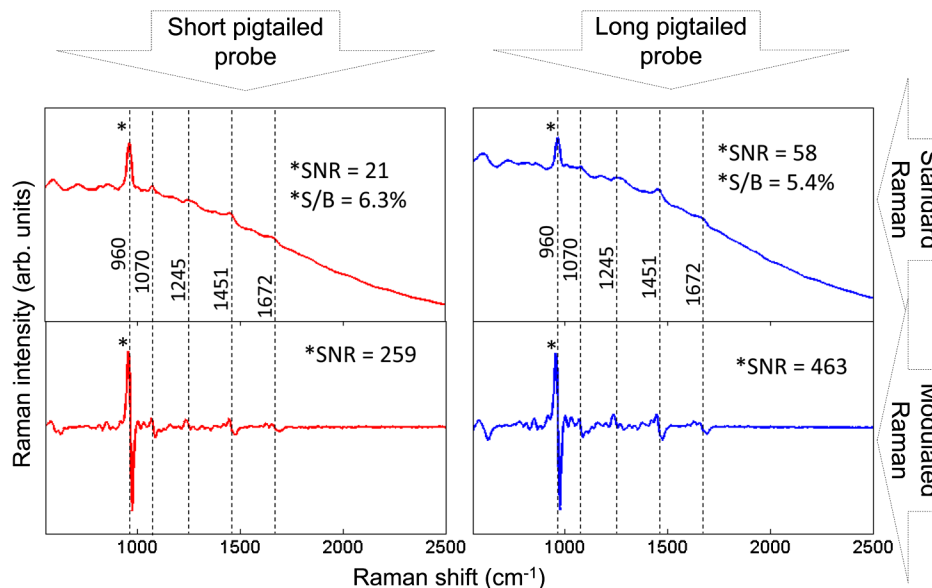

Fig. 2 Comparison between the standard and modulated Raman signal of bovine bone tissue recorded using two fiber probes with different fiber pigtail length. The SNR has been estimated from 20 Raman spectra acquired with a total acquisition time of 30 s each. The modulated Raman spectrum has been obtained by applying PCA to six Raman spectra acquired with single acquisition time of 5 s each. Standard Raman spectrum has been obtained by accumulating six Raman spectra acquired with single acquisition time of 5 s each. (Peak assignment: phosphate ν_1: 960 cm^{-1}, carbonate ν_1: 1070 cm^{-1}, amide III: 1245 cm^{-1}, CH2 scissoring: 1451 cm^{-1}, amide I: 1672 cm^{-1}).
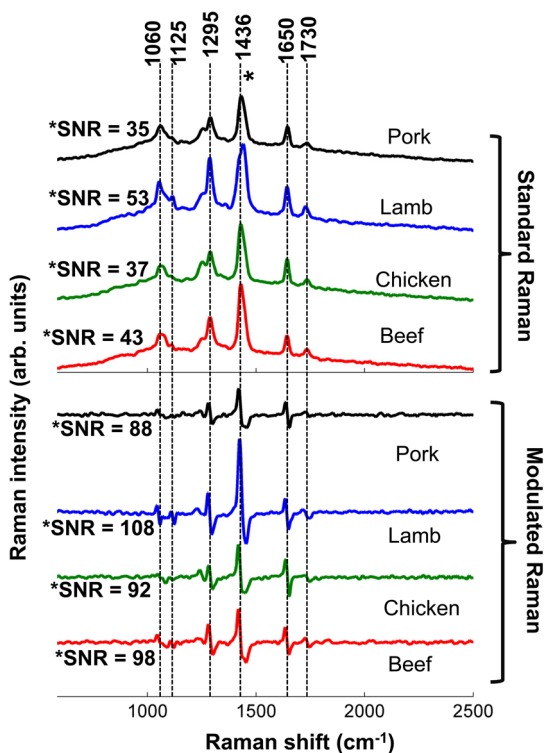
Fig. 3 Comparison between the standard and modulated Raman mean spectra of the adipose tissue from pork, lamb, chicken, and beef. The SNR has been estimated from 20 Raman spectra acquired with a total acquisition time of 30 s each. Modulated Raman spectra have been obtained by applying PCA to six Raman spectra acquired with single acquisition times of 5 s each. Standard Raman spectra were obtained by accumulating six Raman spectra acquired with single acquisition times of 5 s each. (Peak assignment: out-of-phase aliphatic C-C stretch all-trans: 1060 cm^{-1}, in-phase aliphatic C-C stretch all trans: 1125 cm^{-1}, methylene twisting deformations: 1295 cm^{-1}, methylene scissor deformations: 1436 cm^{-1}, olefinic stretch: 1650 cm^{-1}, carbonyl stretch 1730 cm^{-1}).

the SNR has been enhanced by a factor of approximately two when WMRS is implemented.

4 Conclusion

Although fiber-probe-based Raman spectroscopic analysis of tissues is a well-explored technique, the auto-fluorescence of the sample and the fluorescence background from the fiber are some of the issues that need to be considered and which limits the applicability of this technique. We have demonstrated here the suitability of using WMRS for achieving fluorescence suppression and Raman signal enhancement in fiber Raman probes within a reasonable acquisition time of 30 s. Importantly, WMRS is an easily implementable technique in fiber Raman probes as it only requires modification of the laser source and the use of suitable post-processing algorithms. We have shown that it is possible to correct for photo-bleaching of the sample and power fluctuation of the laser source with a simple two-step processing of the signal.

WMRS has been implemented in analyzing the Raman spectra from bone tissue samples, which have high auto-fluorescence. Significant enhancement was observed for Raman peaks when WMRS was implemented, and Raman spectra with a reasonably good SNR could be obtained with just 30-s acquisition time, without any special sample preparation. It was

also demonstrated that WMRS is applicable for different probes. Further it was demonstrated that WMRS enhanced Raman signal when the fiber probe was used for *ex vivo* chemical fingerprinting of various animal fats. When implemented in fiber Raman probe-based tissue analysis, WMRS will be a powerful tool that may lead to the realization of Raman spectroscopy-based early disease diagnosis.

Appendix: Matlab Code for Correcting Power Fluctuation and Photobleaching

```
%% Correction for power fluctuation and photobleaching

% X is an n-by-p matrix, with rows corresponding to pixels (Wavelength)
and columns to spectrum

s2 = size(X, 1);

noise_reg = X(noise_pos − 5 : noise_pos + 5, :);

% noise_pos is a pixel around which noise region is selected

noise_reg = mean(noise_reg);

x = 1 : size(noise_reg, 2);

pr = polyfit(x, noise_reg, 2); %Fitting 2nd order polynomial

p_val = polyval(pr, x);

noise_reg = (noise_reg − p_val) + pr(end); %Subtracting polynomial fit

noise_corr = noise_reg./noise_reg(floor(s1/2)); %Intensity fluctuation
correction factors

X = X./repmat(noise_corr, s2, 1); %Correcting whole dataset for
intensity fluctuations

x = 1 : s1;

for i = 1 : s2

pr = polyfit(x, X(i, :), 3);

p_val = polyval(pr, x);

X(i, :) = (X(i, :) − p_val) + pr(end); % Correcting for photobleaching
effect

end
```

References

1. J. Chan et al., "Raman spectroscopy and microscopy of individual cells and cellular components," *Laser Photon. Res.* **2**(5), 325–349 (2008).
2. H. P. Buschma et al., "*In vivo* determination of the molecular composition of artery wall by intravascular Raman spectroscopy," *Anal. Chem.* **72**(16), 3771–3775 (2000).
3. K. Golcuk et al., "Is photobleaching necessary for Raman imaging of bone tissue using a green laser?," *Biochim. Biophys. Acta* **1758**(7), 868–873 (2006).

4. D. A. Shea and M. D. Morris, "Bone tissue fluorescence reduction for visible laser Raman spectroscopy," *Appl. Spectrosc.* **56**(2), 182–186 (2002).

5. G. Penel, G. Leroy, and E. Bres, "New preparation method of bone samples for Raman microspectrometry," *Appl. Spectrosc.* **52**(2), 312–313 (1998).

6. S. T. McCain, R. M. Willett, and D. J. Brady, "Multi-excitation Raman spectroscopy technique for fluorescence rejection," *Opt. Express* **16**(15), 10975–10991 (2008).

7. S. Bruckner, H. Jeziorowski, and H. Knözinger, "Frequency modulation Raman spectroscopy," *Chem. Phys. Lett.* **105**(2), 218–222 (1984).

8. J. Funfschilling and D. F. Williams, "CW laser wavelength modulation in Raman and site selection fluorescence spectroscopy," *Appl. Spectrosc.* **30**(4), 443–446 (1976).

9. F. L. Galeener, "FM spectroscopy: Raman scattering and luminescence," *Chem. Phys. Lett.* **48**(1), 7–11 (1977).

10. K. H. Levin and C. L. Tang, "Wavelength-modulation Raman spectroscopy," *Appl. Phy. Lett.* **33**(9), 817–819 (1978).

11. R. F. Begley, A. B. Harvey, and R. L. Byer, "Coherent anti-Stokes Raman spectroscopy," *Appl. Phy. Lett.* **25**(7), 387–390 (1974).

12. R. P. Van Duyne, D. L. Jeanmaire, and D. F. Shriver, "Mode-locked laser Raman spectroscopy. New technique for the rejection of interfering background luminescence signals," *Anal. Chem.* **46**(2), 213–222 (1974).

13. M. Mazilu et al., "Optimal algorithm for fluorescence suppression of modulated Raman spectroscopy," *Opt. Express* **18**(11), 11382–11395 (2010).

14. J. T. Motz et al., "Optical fiber probe for biomedical Raman spectroscopy," *App. Opt.* **43**(3), 542–554 (2004).

15. P. C. Ashok et al., "Fiber probe based microfluidic Raman spectroscopy," *Opt. Express* **18**(8), 7642–7649 (2010).

16. J. T. Motz et al., "Real-time Raman system for *in vivo* disease diagnosis," *J. Biomed. Opt.* **10**(3), 031113 (2005).

17. A. Mahadevan-Jansen et al., "Development of a fiber optic probe to measure NIR Raman spectra of cervical tissue *in vivo*," *Photochem. Photobiol.* **68**(3), 427–431 (1998).

18. S. Koljenovic et al., "Tissue characterization using high wave number Raman spectroscopy," *J. Biomed. Opt.* **10**(3), 031116–031111 (2005).

19. M. V. Schulmerich et al., "Subsurface Raman spectroscopy and mapping using a globally illuminated non-confocal fiber-optic array probe in the presence of Raman photon migration," *Appl. Spectrosc.* **60**(2), 109–114 (2006).

20. M. V. Schulmerich et al., "Transcutaneous fiber optic Raman spectroscopy of bone using annular illumination and a circular array of collection fibers," *J. Biomed. Opt.* **11**(6), 060502–060503 (2006).

21. M. V. Schulmerich et al., "Transcutaneous Raman spectroscopy of murine bone *in vivo*," *Appl. Spectrosc.* **63**(3), 286–295 (2009).

22. P. Matousek et al., "Noninvasive Raman Spectroscopy of human tissue *in vivo*," *Appl. Spectrosc.* **60**(7), 758–763 (2006).

23. M. V. Schulmerich et al., "Noninvasive Raman tomographic imaging of canine bone tissue," *J. Biomed. Opt.* **13**(2), 020506–020503 (2008).

24. K. A. Doole et al., "Stress mapping of undamaged, strained, and failed regions of bone using Raman spectroscopy," *J. Biomed. Opt.* **14**(4), 044018–044018 (2009).

25. P. C. Ashok et al., "Enhanced bioanalyte detection in waveguide confined Raman spectroscopy using wavelength modulation," *J. Biophoton.* **4**(7–8), 514–518 (2011).

26. J. Beattie et al., "Prediction of adipose tissue composition using Raman spectroscopy: average properties and individual fatty acids," *Lipids* **41**(3), 287–294 (2006).

27. J. Beattie et al., "Classification of adipose tissue species using Raman spectroscopy," *Lipids* **42**(7), 679–685 (2007).

28. P. C. Ashok et al., "Waveguide confined Raman spectroscopy for microfluidic interrogation," *Lab Chip* **11**(7), 1262–1270 (2011).